Essential role of CFAP53 in sperm flagellum biogenesis

Bingbing Wu [1,8#], Xiaochen Yu [2,3,4,5,6#], Chao Liu[1], Lina Wang[9], Tao Huang[2,3,4,5,6], Gang Lu[2,3,4,5,6,7], Zi-Jiang Chen[2,3,4,5,6,7], Wei Li[1,8*], Hongbin Liu[2,3,4,5,6,7*]

[1] State Key Laboratory of Stem Cell and Reproductive Biology, Institute of Zoology, Chinese Academy of Sciences, Beijing 100101, China

[2]Center for Reproductive Medicine, Cheeloo College of Medicine, Shandong University, Jinan, Shandong, 250012, China

[3]Key laboratory of Reproductive Endocrinology of the Ministry of Education, Shandong University, Jinan, Shandong, 250012, China

[4]Shandong Key Laboratory of Reproductive Medicine, Jinan, Shandong, 250012, China

[5]Shandong Provincial Clinical Research Center for Reproductive Health, Jinan, Shandong, 250012, China

[6]National Research Center for Assisted Reproductive Technology and Reproductive Genetics, Shandong University, Jinan, Shandong, 250012, China

[7]CUHK-SDU Joint Laboratory on Reproductive Genetics, School of Biomedical Sci-ences, the Chinese University of Hong Kong, Hong Kong 999077, China[8]College of Life Sciences, University of Chinese Academy of Sciences, Beijing 100049, China

[9]China National Clinical Research Center of Respiratory Diseases; Respiratory Department of Beijing Children's Hospital, Capital Medical University; National Center for Children's Health, China

[#] These authors contributed equally to this work.

[*]Corresponding Authors:

Dr. Wei Li

leways@ioz.ac.cn

Dr. Hongbin Liu

hongbin_sduivf@aliyun.com

Keywords: male infertility, flagellum, CFAP53, intramanchette transport, intraflagellar transport

Abstract

The sperm flagellum is essential for male fertility. Despite vigorous research progress towards understanding the pathogenesis of flagellum-related diseases, much remains unknown about the mechanisms underlying the flagellum biogenesis itself. Here, we show that the cilia and flagella associated protein 53 (*Cfap53*) gene is predominantly expressed in testes, and it is essential for sperm flagellum biogenesis. The knockout of this gene resulted in complete infertility in male mice but not in the females. CFAP53 localized to the manchette and sperm tail during spermiogenesis, the knockout of this gene impaired flagellum biogenesis. Furthermore, we identified two manchette and sperm tail-associated proteins that interacted with CFAP53 during spermiogenesis. The disruption of *Cfap53* decreased the expression level of these two proteins and disrupted their localization in spermatids. Together, our results suggest that CFAP53 is an essential protein for sperm flagellum biogenesis, and its mutations might be associated with MMAF.

Introduction

Infertility is a widespread human health issue, affecting 10%–15% of couples worldwide, and male factors account for around 50% of these cases (Boivin et al., 2007; Tüttelmann et al., 2018). Male infertility is clinically diagnosed as azoospermia, decreased sperm concentration (oligozoospermia), reduced percentage of morphologically normal sperm (teratozoospermia), or lower sperm motility (asthenozoospermia) (Coutton et al., 2015; Ray et al., 2017; Tüttelmann et al., 2018; Zinaman et al., 2000). Spermatozoa are polarized cells composed of two main parts, the head and the flagellum. The flagellum makes up about 90% of the length of the sperm and is essential for sperm motility (Burgess et al., 2003; Mortimer, 2018), and it contains axoneme and peri-axonemal structures, such as the mitochondrial sheath, outer dense fibers, and the fibrous sheath (Mortimer, 2018), and the presence of these structures allows the flagellum to be divided into the connecting piece, midpiece, principal piece, and endpiece (M. S. Lehti & A. Sironen, 2017). Defects in formation of the flagellum disrupt sperm morphology and motility, leading to male infertility (Chemes & Rawe, 2010; Sironen et al., 2020; Turner et al., 2020). Great progress has been made in our understanding of the pathogenesis of flagella-related diseases in recent years, but the pathogenic genes and mechanisms of flagellum biogenesis are far from being fully understood.

The flagellum needs to be integrated with the head in order to function properly during fertilization, and a very complex structure called the sperm head-tail coupling apparatus (HTCA) is necessary for the integration of the sperm head and the flagellum, and defects in this structure result in acephalic spermatozoa syndrome (Wu et al., 2020). Recently, *SUN5*, *PMFBP1*,

HOOK1, *BRDT*, *TSGA10*, and *CEP112* have been found to be involved in the assembly of the HTCA, and mutations in these genes are associated with acephalic spermatozoa syndrome (Chen et al., 2018; Li et al., 2017; Sha, Wang, et al., 2020; Sha et al., 2018; Shang et al., 2018; Zhu et al., 2018; Zhu et al., 2016). Abnormalities of the axoneme and accessory structures mainly result in asthenozoospermia, which is associated with morphological flagellar defects such as abnormal tails, irregular mitochondrial sheaths, and irregular residual cytoplasm (Escalier & Touré, 2012; Tu et al., 2020). Previous studies have identified several flagella-associated genes, including *AKAP3*, *AKAP4*, *TTC21A*, *TTC29*, *FSIP2*, *DNAH1*, *DNAH2*, *DNAH6*, *DNAH8*, *DNAH17*, and *DZIP1*, that are involved in sperm flagellum biogenesis (Ben Khelifa et al., 2014; Y. Li et al., 2019; C. Liu et al., 2019; C. Liu et al., 2020; W. Liu et al., 2019; Lv et al., 2020; Martinez et al., 2018; Sha, Wei, et al., 2020; Tu et al., 2019; Turner et al., 2001). Mutations in these genes cause multiple morphological abnormalities of the flagella (MMAF), which is characterized as sperm without flagella or with short, coiled, or otherwise irregular flagella (Ben Khelifa et al., 2014; Touré et al., 2020). There are two evolutionarily conserved bidirectional transport platforms that are involved in sperm flagellum biogenesis, including intramanchette transport (IMT) and intraflagellar transport (IFT) (Kierszenbaum, 2001, 2002; San Agustin et al., 2015). IMT and IFT share similar cytoskeletal components, namely microtubules and F-actin, that provide tracks for the transport of structural proteins to the developing tail (Abraham L. Kierszenbaum et al., 2011), and mutations in *TTC21A*, *TTC29*, *SPEF2*, and *CFAP69*, which have been reported to disrupt sperm flagellar protein transport, also lead to MMAF (Dong FN, 2018; C. Liu et al., 2019; Chunyu Liu et al., 2020; W. Liu et al., 2019; Sha et al., 2019).

The cilia and flagella associated protein (CFAP) family, such as *CFAP58*, *CFAP61*, *CFAP69*, *CFAP65*, *CFAP43*, *CFAP44*, *CFAP70*, and *CFAP251*, is associated with flagellum biogenesis and morphogenesis (Beurois et al., 2019; Dong FN, 2018; He et al., 2020; Huang et al., 2020; W. Li et al., 2019; Li et al., 2020; Tang et al., 2017). Previous studies have indicated that the functional role of CFAP53 (also named the coiled-coil domain containing protein CCDC11) is involved in the biogenesis and motility of motile cilia (Narasimhan et al., 2015; Noël et al., 2016; Perles et al., 2012; Silva et al., 2016), and CFAP53 is localized not only to the base of the nodal cilia, but also along the axoneme of the tracheal cilia (Ide et al., 2020). However, the exact localization and function of CFAP53 during spermiogenesis is still poorly understood. In the present study, we used a *Cfap53* knockout mouse model to study the underlying mechanism of CFAP53 in sperm flagellum biogenesis. We demonstrated that CFAP53 is localized to the manchette and the sperm tail of spermatids, and we found that depletion of CFAP53 led to defects in sperm flagellum biogenesis and sperm head shaping. Moreover, we identified two proteins that interacted with CFAP53 during spermiogenesis, namely intraflagellar transport protein 88 (IFT88) and coiled-coil domain containing 42 (CCDC42). *Cfap53* knockout reduced the accumulation of both IFT88 and CCDC42 and disrupted the localization of IFT88 in spermatids. Thus, in addition to uncovering the essential role of CFAP53 in sperm flagellum biogenesis, we also show that CFAP53 might participate in the biogenesis of the sperm flagellum by collaborating with the IMT and IFT pathways.

Results

Cfap53 knockout leads to male infertility

To identify the biological function of CFAP53, we first examined its expression pattern in different tissues and found that it was predominantly expressed in testis (Fig. 1A). Further immunoblotting of mouse testis lysates prepared from different days after birth was carried out. CFAP53 was first detected in testis at postnatal day 7 (P7), and the level increased continuously from postnatal P14 onward, with the highest levels detected in adult testes (Fig. 1B). This time course corresponded with the onset of meiosis, suggesting that CFAP53 might have an essential role in spermatogenesis.

To characterize the potential functions of CFAP53 during spermatogenesis, *Cfap53*$^{-/-}$ mice were created using the CRISPR-Cas9 system from Cyagen Biosciences. Exon 4 to exon 6 of the *Cfap53* gene was selected as the target site (Fig. 1C). The founder animals were genotyped by genomic DNA sequencing and further confirmed by polymerase chain reaction – the total size of the *Cfap53* locus in *Cfap53*$^{+/+}$ mice was 918 bp, while the size of the locus in *Cfap53*$^{-/-}$ mice was 630 bp (Fig. 1D). Immunoblotting of testis indicated that the CFAP53 protein was successfully eliminated in *Cfap53*$^{-/-}$ mice (Fig. 1H). Because we cannot obtain adult homozygous *Cfap53*$^{-/-}$ mice in the C57BL/6J (C57) background, the heterozygous *Cfap53* mutated mice in the C57 background were further crossed with wild-type (WT) ICR mice, and the resulting heterozygotes were interbred to obtain homozygous *Cfap53*$^{-/-}$ mice in the C57/ICR background. The offspring genotypes deviated from Mendelian ratios (115:237:60 for *Cfap53*$^{+/+}$: *Cfap53*$^{+/-}$: *Cfap53*$^{-/-}$), suggesting an increased prenatal lethal rate in *Cfap53*$^{-/-}$ mice. We analyzed 25 *Cfap53*$^{-/-}$ mice, and 48% (12/25) of them presented with situs inversus totalis

(SIT) and nearly 8% (2/25) had situs inversus abdominalis (SIA). In addition, 32% (8/25) of the *Cfap53*$^{-/-}$ mice developed hydrocephalus (Supplementary Fig. 1).

A total of 72% (43/60) of the *Cfap53*$^{-/-}$ mice that survived after birth died within 6 weeks, while 25% (15/60) of the *Cfap53*$^{-/-}$ mice lived longer than 8 weeks of age (Fig. 1E). We further examined the fertility of *Cfap53* male and female knockout mice. *Cfap53* male knockout mice exhibited normal mounting behaviors and produced coital plugs, but *Cfap53*$^{-/-}$ male mice failed to produce any offspring after mating with WT adult female mice. In contrast, *Cfap53*$^{-/-}$ female mice generated offspring after mating with WT males (Fig. 1F–G). Thus, the disruption in *Cfap53* resulted in male infertility but did not affect the fertility of *Cfap53*$^{-/-}$ female mice.

The knockout of *Cfap53* results in MMAF

To further investigate the cause of male infertility, we first observed the adult *Cfap53*$^{-/-}$ testis structure at both the gross and histological levels. The body weight of *Cfap53*$^{-/-}$ male mice was reduced compared to *Cfap53*$^{+/+}$ male mice (Fig. 1J), while there were no significant differences in the testis size, testis weight, or testis/body weight ratio between *Cfap53*$^{-/-}$ and *Cfap53*$^{+/+}$ male mice (Fig. 1I, K, L). We then observed the transverse sections of the *Cfap53*$^{-/-}$ cauda epididymis by hematoxylin and eosin (H&E) staining and found that there was a complete lack of spermatozoa or only a few spermatozoa in the epididymal lumen of *Cfap53*$^{-/-}$ mice (Fig. 2A, red arrowhead). We examined the spermatozoa released from the caudal epididymis and found the sperm count in the *Cfap53*$^{-/-}$ mice to be significantly decreased compared with WT mice (Fig. 2B). To determine the morphological characteristics of the spermatozoa, we performed single-sperm immunofluorescence of lectin peanut agglutinin (PNA), which is used to visualize the acrosomes of spermatozoa. The *Cfap53*$^{-/-}$ caudal epididymis only contained malformed

157 spermatozoa exhibiting the prominent MMAF phenotype of short, coiled, or absent flagella
158 compared with *Cfap53*$^{+/+}$ mice. In addition to the flagella abnormality, *Cfap53*$^{-/-}$ mice had
159 abnormal sperm heads (Fig. 2C). The ratio of spermatozoa with abnormal heads and flagella is
160 shown in Fig. 2D. Abnormal sperm head with short tail and normal sperm head with curly tail
161 were the major defect categories. Immunofluorescence analysis with MitoTracker, which is
162 used to visualize mitochondria, showed that the mitochondrial sheath was malformed in the
163 *Cfap53*$^{-/-}$ spermatozoa (Supplementary Fig. 2).

164 **CFAP53 is required for spermatogenesis**

165 To address the question of why *Cfap53* knockout results in MMAF, we conducted Periodic
166 acid–Schiff (PAS) staining to determine the stages of spermatogenesis in *Cfap53*$^{-/-}$ and WT
167 testes. The most prominent defects were observed in the spermatids at the stages of
168 spermatogenesis, where abnormally elongated and constricted sperm head shapes were
169 identified (Fig. 3A, asterisks). In addition, some dead cells could be detected in the *Cfap53*$^{-/-}$
170 seminiferous tubules (Fig. 3A). To clarify the detailed morphological effects of the *Cfap53*
171 mutation on the structure of sperm heads, we analyzed the process of sperm head shaping
172 between *Cfap53*$^{-/-}$ and *Cfap53*$^{+/+}$ mice. Notably, from step 1 to step 8 the acrosome and nucleus
173 morphology in *Cfap53*$^{-/-}$ spermatids was normal compared with *Cfap53*$^{+/+}$ spermatids. Head
174 shaping started at step 9 to step 10, and the morphology of the elongated *Cfap53*$^{-/-}$ spermatid
175 heads was normal compared with that of *Cfap53*$^{+/+}$ mice, whereas abnormal club-shaped heads
176 (Fig. 3B) were seen in step 11 spermatids in *Cfap53*$^{-/-}$ mice. This phenomenon became more
177 apparent between step 11 and step 16 (Fig. 3B). Taken together, these results indicate that
178 CFAP53 is required for normal spermatogenesis.

H&E staining was used to further observe the morphological changes of the seminiferous tubules. The seminiferous tubules of *Cfap53*$^{+/+}$ mice had a tubular lumen with flagella appearing from the developing spermatids. In contrast, the flagella were absent in the seminiferous tubules of *Cfap53*$^{-/-}$ mice (Fig. 4A). Immunofluorescence staining for α/β-tubulin, the specific flagellum marker, further confirmed the defects in flagellum biogenesis resulting from the knockout of *Cfap53* (Fig. 4B). These observations clearly suggest that CFAP53 plays an important role in flagellum biogenesis.

CFAP53 is required for sperm flagellum biogenesis and correct manchette function

In order to determine the causes of the abnormal sperm morphology in *Cfap53*$^{-/-}$ mice, we investigated the effect of *Cfap53* knockout on flagellum biogenesis using the antibody against acetylated tubulin, a flagellum-specific marker. Unlike the well-defined flagellum of the control group, the axoneme was absent in step 2–3 spermatids in *Cfap53*$^{-/-}$ mice (Fig. 4C, asterisks). In steps 4–6, abnormally formed flagella were seen in *Cfap53*$^{-/-}$ testis sections (Fig. 4C). The presence of long and abnormal spermatid heads suggested defects in the function of the manchette, which is involved in sperm head shaping. Immunofluorescence staining for α/β-tubulin antibody showed that manchette formation was normal in step 8 to step 10 spermatids in *Cfap53*$^{-/-}$ mice, while step 11 to step 13 spermatids of *Cfap53*$^{-/-}$ mice had abnormally long manchettes compared with WT controls. (Fig. 4D). We performed transmission electron microscopy to study the organization of the sperm manchette in detail in *Cfap53*$^{-/-}$ mice. During the chromatin condensation period starting from step 11 spermatids, the manchette of *Cfap53*$^{-/-}$ mice appeared abnormally long and the perinuclear ring constricted the sperm nucleus, causing severe defects in sperm head formation (Fig. 4E). Thus, deletion of *Cfap53* causes

severe defects in sperm flagellum biogenesis and manchette function.

CFAP53 localizes to the manchette and the sperm tail

In order to determine the functional role of CFAP53 during spermiogenesis, we investigated the subcellular localization of CFAP53 during spermatogenesis in mice using an anti-CFAP53 antibody. The CFAP53 signal was first observed as two adjacent dots nearby the nucleus in spermatocytes and early round spermatids (Fig. 5A), and these results were consistent with the protein expression patterns (Fig. 1B). During the elongation of the spermatids (step 9 to step 14), CFAP53 could be detected as a skirt-like structure that encircled the elongating spermatid head, and the protein was subsequently located to the sperm tail around step 14 to step 15. Compared to *Cfap53*$^{+/+}$ mice, there was no CFAP53 staining detected in the germ cells of *Cfap53*$^{-/-}$ male mice (Fig. 5A). To determine whether CFAP53 associates with microtubular structures, the localization of CFAP53 in the elongating and elongated spermatid was subsequently co-stained with antibodies against α-tubulin (a manchette marker) and against CFAP53. In the elongating spermatid CFAP53 colocalized with the manchette microtubules. CFAP53 was further identified at the sperm tail, whereas α-tubulin marked the whole tail in the elongated spermatids (Fig. 5B). Taken together, these results indicate that CFAP53 might participate in manchette formation and flagellum biogenesis.

CFAP53 interacts with IFT88 and CCDC42

Sperm flagellum biogenesis requires protein delivery to the assembly sites via IMT and IFT (Lehti & Sironen, 2016). According to the localization and functional role of CFAP53 during spermiogenesis, some IFT/IMT-related genes were chosen to determine their interactions with

CFAP53 by coimmunoprecipitation (co-IP) assays. IFT88 and IFT20, which belong to the IFT family, are involved in protein transport, and their depletion affects sperm flagellum biogenesis (A. L. Kierszenbaum et al., 2011; Zhang et al., 2016). CCDC42 is involved in IMT and is essential for sperm flagellum biogenesis (Pasek et al., 2016; Tapia Contreras & Hoyer-Fender, 2019). To determine their relationship with CFAP53, HEK293T cells were co-transfected with MYC-tagged CFAP53 and IFT88-GFP, CCDC42-GFP, or GFP-tagged empty vector plasmid as a control, and we found that both IFT88 and CCDC42 were coimmunoprecipitated with CFAP53-MYC (Fig. 6A-C). We did not detect any interaction between IFT20-FLAG and CFAP53-MYC using the same strategy (Fig. 6D). To further determine their relationship, we performed immunoblotting of IFT88 and CCDC42 in the testes of *Cfap53*$^{+/+}$ and *Cfap53*$^{-/-}$ mice, and we found that the expression levels of IFT88 and CCDC42 were significantly reduced in the testes of *Cfap53*$^{-/-}$ mice (Fig. 6E, F). Taken together, we show that CFAP53 interacts with IFT88 and CCDC42 and that the knockout of *Cfap53* decreases the expression of CCDC42 and IFT88.

Both IFT88 and CCDC42 localize to the manchette, the sperm connecting piece, and the sperm tail during spermatogenesis (A. L. Kierszenbaum et al., 2011; Pasek et al., 2016; Tapia Contreras & Hoyer-Fender, 2019). Because the antibody against CCDC42 does not function for immunofluorescence, we focused on IFT88. Similar to the knockout of *Cfap53*, spermatozoa in the *Ift88* mutant mouse had absent, short, or irregular tails with malformed sperm heads (A. L. Kierszenbaum et al., 2011; San Agustin et al., 2015). In order to further investigate the effect of *Cfap53* knockout on IFT88 localization and its potential interaction with CFAP53 during sperm development, we co-stained the differentiating spermatids with

antibodies against IFT88 and CFAP53. We found that IFT88 located to the manchette, the HTCA, and the sperm tail as previously reported (A. L. Kierszenbaum et al., 2011; San Agustin et al., 2015). CFAP53 co-localized with IFT88 in the manchette of the elongating spermatid and in the sperm tail of the elongated spermatid (Fig. 6G). We next detected IFT88 localization in the different steps of spermatid development in *Cfap53*$^{+/+}$ and *Cfap53*$^{-/-}$ mice. The IFT88 signal was first observed in the tail of round spermatids and continued to be detected in the elongated spermatid. Unlike the well-defined flagellum signal of the control group, the detectable IFT88 signal was abnormal in the spermatids of *Cfap53*$^{-/-}$ mice (Fig. 6H). This result suggests that both CFAP53 and IFT88 might cooperatively participate in flagellum biogenesis during spermiogenesis.

Discussion

In this study, we have identified the essential role of CFAP53 in spermatogenesis and male fertility by generating *Cfap53*$^{-/-}$ mice with the deletion of exons 4–6. Sperm flagellum biogenesis begins in early round spermatids, where the axoneme extends from the distal centriole (Mari S Lehti & Anu Sironen, 2017). It has been reported that the expression of many genes that are necessary for sperm flagellum biogenesis is significantly increased at approximately 12 days after birth (Horowitz et al., 2005), and we found that CFAP53 expression was upregulated in the testes between 7 and 14 days after birth (Fig. 1B), which was consistent with the timing of axoneme formation. Previous studies have shown that CFAP53 is located at the basal body and on centriolar satellites in retinal pigment epithelial cells and on the ciliary axonemes in zebrafish kidneys and human respiratory cells (Narasimhan et al., 2015;

Silva et al., 2016). In mice, CFAP53 is located at the base of the nodal cilia and the tracheal cilia, as well as along the axonemes of the tracheal cilia (Ide et al., 2020). Depletion of CFAP53 disrupts the subcellular organization of satellite proteins and lead to primary cilium assembly abnormalities (Silva et al., 2016), and knockout of CFAP53 disrupts ciliogenesis in human tracheal epithelial multiciliated cells, in *Xenopus* epidermal multiciliated cells, and in zebrafish Kupffer's vesicle and pronephros (Narasimhan et al., 2015; Noël et al., 2016; Silva et al., 2016). The mammalian sperm flagellum contains an axoneme composed of a 9+2 microtubule arrangement, which is similar to that of motile cilia. Our study further showed that axoneme formation was impaired in early round spermatids in *Cfap53*$^{-/-}$ mice (Fig. 4C), thus demonstrating that CFAP53 is essential for sperm flagellum biogenesis.

We found that CFAP53 localized on the manchette and tail during spermiogenesis, and it could interact with IFT88 and CCDC42, both of which colocalized to the same positions during spermiogenesis (Fig. 6A, B, G). In addition, it has been reported that CFAP53 also interacts with KIF3A in adult testis (Lehti et al., 2013). All of these partner proteins are related to manchette and flagellum biogenesis, with the manchette being one of the transient skirt-like microtubular structures that are required for the formation of sperm flagella and the shaping of the head during spermatid elongation (Kierszenbaum & Tres, 2004; Lehti & Sironen, 2016). It has been proposed that flagellar structure proteins and motor proteins are transported through the manchette via IMT to the base of the sperm flagellum and via IFT to the developing sperm flagellum (Abraham L. Kierszenbaum et al., 2011; Lehti & Sironen, 2016). Both IMT and IFT provide the bidirectional movement of multicomponent transport systems powered by molecular motors along the microtubules, and both are essential for axoneme assembly (Mari

S Lehti & Anu Sironen, 2017). Molecular motors (kinesin-2 and dynein 2) move cargo proteins associated with protein rafts consisting of IFT proteins (Chien et al., 2017; Kierszenbaum, 2002; Zhu et al., 2020), and KIF3A, the motor subunit of kinesin-2, works as an anterograde motor for transporting IFT complex B during the development of the sperm tail (Lehti et al., 2013; Marszalek JR, 1999). KIF3A localizes to the manchette, the basal body, and the axoneme of spermatids, and disruption of KIF3A affects the formation of the manchette and further disrupts the delivery of proteins to the sperm tail (Lehti et al., 2013). IFT88 is an IFT complex B protein that is regarded as a member of the IMT machinery. Notably, the reproductive phenotype of *Ift88* knockout male mice was similar to what we observed in *Cfap53* knockout mice (San Agustin et al., 2015). Thus, CFAP53 might function in collaboration with IFT88 and KIF3A in flagellum biogenesis via IMT and IFT (Fig. 7).

Previous studies have shown that *Ccdc42* knockout male mice have abnormal head shapes and axoneme assembly defects, and it was speculated that CCDC42 might be a passenger protein transported via the manchette towards the developing tail (Pasek et al., 2016; Tapia Contreras & Hoyer-Fender, 2019). As a partner protein of CCDC42 and IFT88, once CFAP53 was depleted the expression levels of these two partner proteins were also decreased significantly (Fig 6E, F). These results raise the question of whether CFAP53 works as a cargo protein or as a component of the IFT and IMT machineries. Given that CFAP53 also localized on sperm flagella, we are drawn to the conclusion that CFPA53 works as a cargo protein and that and it might be involved in the stabilization of other cargo proteins, such as CCDC42, that are transported by IFT and IMT (Fig 7). As for the decreasing of IFT88, this is likely caused by the decreasing demand for cargo protein transportation via IMT and IFT to the developing

sperm tail. Accordingly, our current conclusions can be further expanded to other flagellum-associated proteins, and the depletion of some cargo proteins that need to be transported by either IMT or IFT should have similar phenotypes due to flagellum biogenesis defects, and at least some of the MMAF might be caused by this mechanism.

Methods

Animals

The mouse *Cfap53* gene (Transcript: ENSMUSG00000035394) is 96.90 kb and contains 8 exons and is located on chromosome 18. Exon 4 to exon 6 was chosen as the target site, and *Cfap53*$^{-/-}$ mice were generated using the CRISPR-Cas9 system from Cyagen Biosciences. The gRNA and Cas9 mRNA were co-injected into fertilized eggs of C57BL/6 mice to generate a targeted line with a 3243 bp base deletion, AAG GTT TGA TCC GAA GTC AT – 3243 bp – CAA GGT TTA AGA ACA GTG TG. The founder animals were genotyped by genomic DNA sequencing. For *Cfap53*$^{-/-}$ mice, the specific primers were Forward: 5'-GAG GGA ATA GGT TTC TGG GTA GGT G-3' and Reverse: 5'-ACC CTT CTG GTC CCT CAG TCA TCT-3', yielding a 630 bp fragment. For *Cfap53* wild-type mice, the specific primers were Forward: 5'-GAG GGA ATA GGT TTC TGG GTA GG TG-3' and Reverse: 5'-AGC AGC AGT GAA ACT TCA AAC ATG G-3', yielding a 918 bp fragment. All of the animal experiments were performed according to approved institutional animal care and use committee (IACUC) protocols (#08-133) of the Institute of Zoology, Chinese Academy of Sciences.

Plasmids

Mouse *Cfap53* was obtained from mouse testis cDNA and cloned into the pCMV-Myc vector using the Clon Express Ultra One Step Cloning Kit (C115, Vazyme). Mouse *Ccdc42* and *Ift88*

were obtained from mouse testis cDNA and cloned into the pEGFP-C1 vector using the Clon Express Ultra One Step Cloning Kit (C115, Vazyme). Mouse *Ift20* was obtained from mouse testis cDNA and cloned into the pRK vector using the Clon Express Ultra One Step Cloning Kit (C115, Vazyme).

Antibodies

Mouse anti-CFAP53 polyclonal antibody (aa 216–358) was generated by Quan Biotech (Wuhan, China) and was used at a 1:10 dilution for immunofluorescence and 1:200 dilution for western blotting. Mouse anti-GFP antibody (1:1000 dilution, M20004L, Abmart, Shanghai, China), rabbit anti-MYC antibody (1:1000 dilution, BE2011, EASYBIO, Beijing, China), mouse anti-FLAG antibody (1:1000 dilution, F1804, Sigma, Shanghai, China), and rabbit anti-CCDC42 antibody (1:500 dilution, abin2785068, antibodies-online, Beijing, China) were used for western blotting. Rabbit anti-α-tubulin antibody (AC007, ABclonal, Wuhan, China) was used at a 1:100 dilution for immunofluorescence and at a 1:10000 dilution for western blotting. IFT88 polyclonal antibody (13967-1-AP, Proteintech, Wuhan, China) was used at a 1:50 dilution for immunofluorescence and at a 1:1000 dilution for western blotting. Mouse anti-α/β-tubulin antibody (1:100, ab44928, Abcam, Shanghai, China) and mouse anti-acetylated-a-tubulin antibody (T7451, 1:1000 dilution, Sigma) were used for immunofluorescence. The secondary antibodies were goat anti-rabbit FITC (1:200, ZF-0311, Zhong Shan Jin Qiao, Beijing, China), goat anti-rabbit TRITC (1:200 dilution, ZF-0316, Zhong Shan Jin Qiao), goat anti-mouse FITC (1:200 dilution, ZF-0312, Zhong Shan Jin Qiao), and goat anti-mouse TRITC (1:200 dilution, ZF-0313, Zhong Shan Jin Qiao). The Alexa Fluor 488 conjugate of lectin PNA (1:400 dilution, L21409, Thermo Fisher Scientific, Shanghai, China) and MitoTracker Deep

353 Red 633 (1:1500 dilution, M22426, Thermo Fisher Scientific) were used for
354 immunofluorescence.

355 **Immunoprecipitation**

356 Transfected HEK293T cells were lysed in ELB buffer (50 mM HEPES, 250 mM NaCl, 0.1%
357 NP-40, 1 mM PMSF, and complete EDTA-free protease inhibitor cocktail (Roche)) for 30 min
358 on ice and centrifuged at 12000 × *g* for 15 min. For immunoprecipitation, cell lysates were
359 incubated with anti-GFP antibody overnight at 4°C and then incubated with protein A-
360 Sepharose (GE, 17-1279-03) for 3 hours at 4°C Thereafter, the precipitants were washed four
361 times with ELB buffer, and the immune complexes were eluted with sample buffer containing
362 1% SDS for 10 min at 95°C and analyzed by immunoblotting.

363 **Immunoblotting**

364 Proteins obtained from lysates or immunoprecipitates were separated by SDS-PAGE and
365 electrotransferred onto a nitrocellulose membrane. The membrane was blocked in 5% skim
366 milk (BD, 232100) and then incubated with corresponding primary antibodies and detected by
367 Alexa Fluor 680 or 800-conjugated goat anti-mouse or Alexa Fluor 680 or 800-conjugated goat
368 anti-rabbit secondary antibodies. Finally, they were scanned using the ODYSSEY Sa Infrared
369 Imaging System (LI-COR Biosciences, Lincoln, NE, RRID:SCR_014579).

370 **Mouse sperm collection**

371 The caudal epididymides were dissected from the *Cfap53* wildtype and knockout mice.
372 Spermatozoa were squeezed out from the caudal epididymis and released in 1 ml phosphate
373 buffered saline (PBS) for 30 min at 37°C under 5% CO_2 for sperm counting and
374 immunofluorescence experiments.

Tissue collection and histological analysis

The testes and caudal epididymides from at least five *Cfap53* wildtype and five knockout mice were dissected immediately after euthanasia. All samples were immediately fixed in 4% (mass/vol) paraformaldehyde (PFA; Solarbio, P1110) for up to 24 hours, dehydrated in 70% (vol/vol) ethanol, and embedded in paraffin. For histological analysis, the 5 μm sections were mounted on glass slides and stained with H&E. For PAS staining, testes were fixed with Bouin's fixatives (Polysciences). Slides were stained with PAS and H&E after deparaffinization, and the stages of the seminiferous epithelium cycle and spermatid development were determined.

Immunofluorescence of the testicular germ cells

The mouse testis was immediately dissected and fixed with 2% paraformaldehyde in 0.05% PBST (PBS with 0.05% Triton X-100) at room temperature for 5 min. The fixed sample was placed on a slide glass and squashed by placing a cover slip on top and pressing down. The sample was immediately flash frozen in liquid nitrogen, and the slides were stored at −80°C for further immunofluorescence experiments (Wellard et al., 2018). After removing the coverslips, the slides were washed with PBS three times and then treated with 0.1% Triton X-100 for 10 min, rinsed three times in PBS, and blocked with 5% bovine serum albumin (Amresco, AP0027). The primary antibody was added to the sections and incubated at 4°C overnight, followed by incubation with the secondary antibody. The nuclei were stained with DAPI. The immunofluorescence images were taken immediately using an LSM 780 microscope (Zeiss) or SP8 microscope (Leica).

Immunofluorescence in testes

The testes of *Cfap53* wildtype and knockout mice were fixed in 4% PFA at 4°C overnight,

dehydrated in 70% (vol/vol) ethanol, and embedded in paraffin. For histological analysis, the 5 μm sections were mounted on glass slides, then deparaffinized and rehydrated, followed by antigen retrieval in 10 mM sodium citrate buffer (pH 6.0) for 15 min and washing three times in PBS, pH 7.4. After blocking with 5% BSA containing 0.1% Triton X-100, the primary antibodies were added to the sections and incubated at 4°C overnight, followed by incubation with the secondary antibody. The nuclei were stained with DAPI, and images were acquired on an SP8 microscope (Leica).

Transmission electron microscopy

The testes from at least three *Cfap53* wildtype and knockout mice were dissected and pre-fixed in 2.5% (vol/vol) glutaraldehyde in 0.1 M cacodylate buffer at 4°C overnight. After washing in 0.1 M cacodylate buffer, samples were cut into small pieces of approximately 1 mm^3, then immersed in 1% OsO_4 for 1 hour at 4°C. Samples were dehydrated through a graded acetone series and embedded in resin for staining. Ultrathin sections were cut on an ultramicrotome and double stained with uranyl acetate and lead citrate, and images were acquired and analyzed using a JEM-1400 transmission electron microscope.

Statistical analysis

All of the experiments were repeated at least three times, and the results are presented as the mean ± SD. The statistical significance of the differences between the mean values for the different genotypes was measured by the Student's t-test with a paired, 2-tailed distribution. The data were considered significant for $P < 0.05$.

Contributors

W.L. and H.B.L. designed the study and wrote the article. B.B.W. performed most of the

419 experiments and analyzed the data. X.C.Y. performed the experiments and assisted in writing
420 the manuscript. C.L., L.N.W., and X.H.L. performed some of the immunofluorescence
421 experiments. All authors assisted in data collection, interpreted the data, provided critical input
422 to the manuscript, and approved the final manuscript.

423 **Acknowledgements**

424 This work was funded by the National Natural Science Foundation of China (grant 81925015),
425 the Strategic Priority Research Program of the Chinese Academy of Sciences (grant
426 XDA16020701) and Qilu Young Scholars Program of Shandong University. We would like to
427 thank the State Key Laboratory of Membrane Biology, Institute of Zoology, Chinese Academy
428 of Science, for our electron microscopy work, and we are grateful to Pengyan Xia for his help
429 in preparing the electron microscopy sample.

430 **Conflicts of interest**

431 The authors declare no conflicts of interest with the contents of this article.

432 **References**

433 Ben Khelifa, M., Coutton, C., Zouari, R., Karaouzène, T., Rendu, J., Bidart, M., Yassine, S.,
434 Pierre, V., Delaroche, J., Hennebicq, S., Grunwald, D., Escalier, D., Pernet-Gallay, K., Jouk, P.
435 S., Thierry-Mieg, N., Touré, A., Arnoult, C., & Ray, P. F. (2014). Mutations in DNAH1, which
436 encodes an inner arm heavy chain dynein, lead to male infertility from multiple morphological
437 abnormalities of the sperm flagella. *Am J Hum Genet* *94*(1), 95-104.
438 https://doi.org/10.1016/j.ajhg.2013.11.017

439 Beurois, J., Martinez, G., Cazin, C., Kherraf, Z.-E., Amiri-Yekta, A., Thierry-Mieg, N., Bidart,
440 M., Petre, G., Satre, V., & Brouillet, S. J. H. R. (2019). CFAP70 mutations lead to male

441 infertility due to severe astheno-teratozoospermia. A case report *34*(10), 2071-2079.
442 https://doi.org/10.1093/humrep/dez166

443 Boivin, J., Bunting, L., Collins, J. A., & Nygren, K. G. (2007). International estimates of
444 infertility prevalence and treatment-seeking: potential need and demand for infertility medical
445 care. *Hum Reprod 22*(6), 1506-1512. https://doi.org/10.1093/humrep/dem046

446 Burgess, S. A., Walker, M. L., Sakakibara, H., Knight, P. J., & Oiwa, K. J. N. (2003). Dynein
447 structure and power stroke. *Nature 421*(6924), 715-718. https://doi.org/10.1038/nature01377

448 Chemes, H. E., & Rawe, V. Y. (2010). The making of abnormal spermatozoa: cellular and
449 molecular mechanisms underlying pathological spermiogenesis. *Cell Tissue Res 341*(3), 349-
450 357. https://doi.org/10.1007/s00441-010-1007-3

451 Chen, H., Zhu, Y., Zhu, Z., Zhi, E., Lu, K., Wang, X., Liu, F., Li, Z., & Xia, W. (2018).
452 Detection of heterozygous mutation in hook microtubule-tethering protein 1 in three patients
453 with decapitated and decaudated spermatozoa syndrome. *J Med Genet 55*(3), 150-157.
454 https://doi.org/10.1136/jmedgenet-2016-104404

455 Chien, A., Shih, S. M., Bower, R., Tritschler, D., Porter, M. E., & Yildiz, A. (2017). Dynamics
456 of the IFT machinery at the ciliary tip. *Elife*, 6. https://doi.org/10.7554/eLife.28606

457 Coutton, C., Escoffier, J., Martinez, G., Arnoult, C., & Ray, P. F. (2015). Teratozoospermia:
458 spotlight on the main genetic actors in the human. *Hum Reprod Update 21*(4), 455-485.
459 https://doi.org/10.1093/humupd/dmv020

460 Dong FN, A.-Y. A., Martinez G, Saut A, Tek J, Stouvenel L, Lorès P, Karaouzène T, Thierry-
461 Mieg N, Satre V, Brouillet S, Daneshipour A, Hosseini SH, Bonhivers M, Gourabi H, Dulioust
462 E, Arnoult C, Touré A, Ray PF, Zhao H, Coutton C. (2018). Absence of CFAP69 causes male

463 infertility due to multiple morphological abnormalities of the flagella in human and mouse. *The*
464 *American Journal of Human Genetics 102*(4), 636-648.
465 https://doi.org/10.1016/j.ajhg.2018.03.007
466 Escalier, D., & Touré, A. (2012). Morphological defects of sperm flagellum implicated in
467 human male infertility. *Med Sci (Paris) 28*(5), 503-511.
468 https://doi.org/10.1051/medsci/2012285015
469 He, X., Liu, C., Yang, X., Lv, M., Ni, X., Li, Q., Cheng, H., Liu, W., Tian, S., Wu, H., Gao, Y.,
470 Yang, C., Tan, Q., Cong, J., Tang, D., Zhang, J., Song, B., Zhong, Y., Li, H., Zhi, W., Mao, X.,
471 Fu, F., Ge, L., Shen, Q., Zhang, M., Saiyin, H., Jin, L., Xu, Y., Zhou, P., Wei, Z., Zhang, F., &
472 Cao, Y. (2020). Bi-allelic Loss-of-function Variants in CFAP58 Cause Flagellar Axoneme and
473 Mitochondrial Sheath Defects and Asthenoteratozoospermia in Humans and Mice. *Am J Hum*
474 *Genet 107*(3), 514-526. https://doi.org/10.1016/j.ajhg.2020.07.010
475 Horowitz, E., Zhang, Z., Jones, B. H., Moss, S. B., Ho, C., Wood, J. R., Wang, X., Sammel, M.
476 D., & Strauss, J. F., 3rd. (2005). Patterns of expression of sperm flagellar genes: early
477 expression of genes encoding axonemal proteins during the spermatogenic cycle and shared
478 features of promoters of genes encoding central apparatus proteins. *Mol Hum Reprod 11*(4),
479 307-317. https://doi.org/10.1093/molehr/gah163
480 Huang, T., Yin, Y., Liu, C., Li, M., Yu, X., Wang, X., Zhang, H., Muhammad, T., Gao, F., Li,
481 W., Zijiang, C., Hongbin, L., & Jinlong, M. (2020). Absence of murine CFAP61 causes male
482 infertility due to multiple morphological abnormalities of the flagella. *Science Bulletin*
483 https://doi.org/10.1016
484 Ide, T., Twan, W. K., Lu, H., Ikawa, Y., Lim, L. X., Henninger, N., Nishimura, H., Takaoka,

485 K., Narasimhan, V., Yan, X., Shiratori, H., Roy, S., & Hamada, H. (2020). CFAP53 regulates
486 mammalian cilia-type motility patterns through differential localization and recruitment of
487 axonemal dynein components. *PLoS Genet 16*(12), e1009232.
488 https://doi.org/10.1371/journal.pgen.1009232
489 Kierszenbaum, A. L. (2001). Spermatid manchette: plugging proteins to zero into the sperm
490 tail. *Mol Reprod Dev 59*(4), 347-349. https://doi.org/10.1002/mrd.1040
491 Kierszenbaum, A. L. (2002). Intramanchette transport (IMT): managing the making of the
492 spermatid head, centrosome, and tail. *Mol Reprod Dev 63*(1), 1-4.
493 https://doi.org/10.1002/mrd.10179
494 Kierszenbaum, A. L., Rivkin, E., & Tres, L. L. (2011). Cytoskeletal track selection during cargo
495 transport in spermatids is relevant to male fertility. *Spermatogenesis 1*(3), 221-230.
496 https://doi.org/10.4161/spmg.1.3.18018
497 Kierszenbaum, A. L., Rivkin, E., Tres, L. L., Yoder, B. K., Haycraft, C. J., Bornens, M., &
498 Rios, R. M. (2011). GMAP210 and IFT88 are present in the spermatid golgi apparatus and
499 participate in the development of the acrosome-acroplaxome complex, head-tail coupling
500 apparatus and tail. *Dev Dyn 240*(3), 723-736. https://doi.org/10.1002/dvdy.22563
501 Kierszenbaum, A. L., & Tres, L. L. (2004). The acrosome-acroplaxome-manchette complex
502 and the shaping of the spermatid head. *Arch Histol Cytol 67*(4), 271-284.
503 https://doi.org/10.1679/aohc.67.271
504 Lehti, M. S., Kotaja, N., & Sironen, A. (2013). KIF3A is essential for sperm tail formation and
505 manchette function. *Mol Cell Endocrinol 377*(1-2), 44-55.
506 https://doi.org/10.1016/j.mce.2013.06.030

Lehti, M. S., & Sironen, A. (2016). Formation and function of the manchette and flagellum during spermatogenesis. *Reproduction 151*(4), R43-54. https://doi.org/10.1530/REP-15-0310

Lehti, M. S., & Sironen, A. (2017). Formation and function of sperm tail structures in association with sperm motility defects. *Biol. Reprod 97*(4), 522-536. https://doi.org/10.1093/biolre/iox096

Li, L., Sha, Y., Wang, X., Li, P., Wang, J., Kee, K., & Wang, B. (2017). Whole-exome sequencing identified a homozygous BRDT mutation in a patient with acephalic spermatozoa. *Oncotarget 8*(12), 19914-19922. https://doi.org/10.18632/oncotarget.15251

Li, W., He, X., Yang, S., Liu, C., Wu, H., Liu, W., Lv, M., Tang, D., Tan, J., & Tang, S. (2019). Biallelic mutations of CFAP251 cause sperm flagellar defects and human male infertility. *Journal of human genetics 64*(1), 49-54. https://doi.org/10.1038/s10038-018-0520-1

Li, W., Wu, H., Li, F., Tian, S., Kherraf, Z.-E., Zhang, J., Ni, X., Lv, M., Liu, C., & Tan, Q. (2020). Biallelic mutations in CFAP65 cause male infertility with multiple morphological abnormalities of the sperm flagella in humans and mice. *J Med Genet 57*(2), 89-95. https://doi.org/10.1136/jmedgenet-2019-106344

Li, Y., Sha, Y., Wang, X., Ding, L., Liu, W., Ji, Z., Mei, L., Huang, X., Lin, S., Kong, S., Lu, J., Qin, W., Zhang, X., Zhuang, J., Tang, Y., & Lu, Z. (2019). DNAH2 is a novel candidate gene associated with multiple morphological abnormalities of the sperm flagella. *Clin Genet 95*(5), 590-600. https://doi.org/10.1111/cge.13525

Liu, C., He, X., Liu, W., Yang, S., Wang, L., Li, W., Wu, H., Tang, S., Ni, X., Wang, J., Gao, Y., Tian, S., Zhang, L., Cong, J., Zhang, Z., Tan, Q., Zhang, J., Li, H., Zhong, Y., Lv, M., Li, J., Jin, L., Cao, Y., & Zhang, F. (2019). Bi-allelic Mutations in TTC29 Cause Male Subfertility

529 with Asthenoteratospermia in Humans and Mice. *Am J Hum Genet 105*(6), 1168-1181.
530 https://doi.org/10.1016/j.ajhg.2019.10.010

531 Liu, C., Lv, M., He, X., Zhu, Y., Amiri-Yekta, A., Li, W., Wu, H., Kherraf, Z.-E., Liu, W., &
532 Zhang, J. (2020). Homozygous mutations in SPEF2 induce multiple morphological
533 abnormalities of the sperm flagella and male infertility. *Journal of Medical Genetics 57*(1), 31-
534 37. https://doi.org/10.1136/jmedgenet-2019-106011

535 Liu, C., Miyata, H., Gao, Y., Sha, Y., Tang, S., Xu, Z., Whitfield, M., Patrat, C., Wu, H.,
536 Dulioust, E., Tian, S., Shimada, K., Cong, J., Noda, T., Li, H., Morohoshi, A., Cazin, C.,
537 Kherraf, Z. E., Arnoult, C., Jin, L., He, X., Ray, P. F., Cao, Y., Touré, A., Zhang, F., & Ikawa,
538 M. (2020). Bi-allelic DNAH8 Variants Lead to Multiple Morphological Abnormalities of the
539 Sperm Flagella and Primary Male Infertility. *Am J Hum Genet 107*(2), 330-341.
540 https://doi.org/10.1016/j.ajhg.2020.06.004

541 Liu, W., He, X., Yang, S., Zouari, R., Wang, J., Wu, H., Kherraf, Z. E., Liu, C., Coutton, C.,
542 Zhao, R., Tang, D., Tang, S., Lv, M., Fang, Y., Li, W., Li, H., Zhao, J., Wang, X., Zhao, S.,
543 Zhang, J., Arnoult, C., Jin, L., Zhang, Z., Ray, P. F., Cao, Y., & Zhang, F. (2019). Bi-allelic
544 Mutations in TTC21A Induce Asthenoteratospermia in Humans and Mice. *Am J Hum Genet*
545 *104*(4), 738-748. https://doi.org/10.1016/j.ajhg.2019.02.020

546 Lv, M., Liu, W., Chi, W., Ni, X., Wang, J., Cheng, H., Li, W.-Y., Yang, S., Wu, H., & Zhang,
547 J. (2020). Homozygous mutations in DZIP1 can induce asthenoteratospermia with severe
548 MMAF. *J Med Genet* https://doi.org/10.1136/jmedgenet-2019-106479

549 Marszalek JR, R.-L. P., Roberts E, Chien KR, Goldstein LS. (1999). Situs inversus and
550 embryonic ciliary morphogenesis defects in mouse mutants lacking the KIF3A subunit of

551 kinesin-II. *Proceedings of the National Academy of Sciences 96*(9), 5043-5048.
552 https://doi.org/10.1073/pnas.96.9.5043

553 Martinez, G., Kherraf, Z. E., Zouari, R., Fourati Ben Mustapha, S., Saut, A., Pernet-Gallay, K.,
554 Bertrand, A., Bidart, M., Hograindleur, J. P., Amiri-Yekta, A., Kharouf, M., Karaouzène, T.,
555 Thierry-Mieg, N., Dacheux-Deschamps, D., Satre, V., Bonhivers, M., Touré, A., Arnoult, C.,
556 Ray, P. F., & Coutton, C. (2018). Whole-exome sequencing identifies mutations in FSIP2 as a
557 recurrent cause of multiple morphological abnormalities of the sperm flagella. *Hum Reprod*
558 *33*(10), 1973-1984. https://doi.org/10.1093/humrep/dey264

559 Mortimer, D. (2018). The functional anatomy of the human spermatozoon: relating
560 ultrastructure and function. *Mol. Hum. Reprod 24*(12), 567-592.
561 https://doi.org/10.1093/molehr/gay040

562 Narasimhan, V., Hjeij, R., Vij, S., Loges, N. T., Wallmeier, J., Koerner-Rettberg, C., Werner,
563 C., Thamilselvam, S. K., Boey, A., Choksi, S. P., Pennekamp, P., Roy, S., & Omran, H. (2015).
564 Mutations in CCDC11, which encodes a coiled-coil containing ciliary protein, causes situs
565 inversus due to dysmotility of monocilia in the left-right organizer. *Hum Mutat 36*(3), 307-318.
566 https://doi.org/10.1002/humu.22738

567 Noël, E. S., Momenah, T. S., Al-Dagriri, K., Al-Suwaid, A., Al-Shahrani, S., Jiang, H.,
568 Willekers, S., Oostveen, Y. Y., Chocron, S., Postma, A. V., Bhuiyan, Z. A., & Bakkers, J.
569 (2016). A Zebrafish Loss-of-Function Model for Human CFAP53 Mutations Reveals Its
570 Specific Role in Laterality Organ Function. *Human Mutation 37*(2), 194-200.
571 https://doi.org/10.1002/humu.22928

572 Pasek, R. C., Malarkey, E., Berbari, N. F., Sharma, N., Kesterson, R. A., Tres, L. L.,

573 Kierszenbaum, A. L., & Yoder, B. K. (2016). Coiled-coil domain containing 42 (Ccdc42) is
574 necessary for proper sperm development and male fertility in the mouse. *Dev. Biol* *412*(2),
575 208-218. https://doi.org/10.1016/j.ydbio.2016.01.042
576 Perles, Z., Cinnamon, Y., Ta-Shma, A., Shaag, A., Einbinder, T., Rein, A. J. J. T., & Elpeleg,
577 O. (2012). A human laterality disorder associated with recessive CCDC11 mutation. *J Med*
578 *Genet*, *49*(6) 386-390. https://doi.org/10.1136/jmedgenet-2011-100457
579 Ray, P. F., Toure, A., Metzler-Guillemain, C., Mitchell, M. J., Arnoult, C., & Coutton, C.
580 (2017). Genetic abnormalities leading to qualitative defects of sperm morphology or function.
581 *Clin Genet 91*(2), 217-232. https://doi.org/10.1111/cge.12905
582 San Agustin, J. T., Pazour, G. J., & Witman, G. B. (2015). Intraflagellar transport is essential
583 for mammalian spermiogenesis but is absent in mature sperm. *Mol Biol Cell* *26*(24), 4358-
584 4372. https://doi.org/10.1091/mbc.E15-08-0578
585 Sha, Y., Liu, W., Wei, X., Zhu, X., Luo, X., Liang, L., & Guo, T. (2019). Biallelic mutations
586 in Sperm flagellum 2 cause human multiple morphological abnormalities of the sperm flagella
587 (MMAF) phenotype. *Clin Genet 96*(5), 385-393. https://doi.org/10.1111/cge.13602
588 Sha, Y., Wang, X., Yuan, J., Zhu, X., Su, Z., Zhang, X., Xu, X., & Wei, X. (2020). Loss-of-
589 function mutations in centrosomal protein 112 is associated with human acephalic spermatozoa
590 phenotype. *Clin Genet 97*(2), 321-328. https://doi.org/10.1111/cge.13662
591 Sha, Y., Wei, X., Ding, L., Mei, L., Huang, X., Lin, S., Su, Z., Kong, L., Zhang, Y., & Ji, Z.
592 (2020). DNAH17 is associated with asthenozoospermia and multiple morphological
593 abnormalities of sperm flagella. *Ann Hum Genet* *84*(3), 271-279.
594 https://doi.org/10.1111/ahg.12369

595 Sha, Y. W., Sha, Y. K., Ji, Z. Y., Mei, L. B., Ding, L., Zhang, Q., Qiu, P. P., Lin, S. B., Wang,
596 X., Li, P., Xu, X., & Li, L. (2018). TSGA10 is a novel candidate gene associated with acephalic
597 spermatozoa. *Clin. Genet 93*(4), 776-783. https://doi.org/10.1111/cge.13140
598 Shang, Y., Yan, J., Tang, W., Liu, C., Xiao, S., Guo, Y., Yuan, L., Chen, L., Jiang, H., Guo, X.,
599 Qiao, J., & Li, W. (2018). Mechanistic insights into acephalic spermatozoa syndrome-
600 associated mutations in the human SUN5 gene. *J Biol Chem 293*(7), 2395-2407.
601 https://doi.org/10.1074/jbc.RA117.000861
602 Silva, E., Betleja, E., John, E., Spear, P., Moresco, J. J., Zhang, S., Yates, J. R., Mitchell, B. J.,
603 & Mahjoub, M. R. (2016). Ccdc11 is a novel centriolar satellite protein essential for ciliogenesis
604 and establishment of left-right asymmetry. *Mol. Biol. Cell 27*(1), 48-63.
605 https://doi.org/10.1091/mbc.E15-07-0474
606 Sironen, A., Shoemark, A., Patel, M., Loebinger, M. R., & Mitchison, H. M. (2020). Sperm
607 defects in primary ciliary dyskinesia and related causes of male infertility. *Cell Mol Life Sci*
608 *77*(11), 2029-2048. https://doi.org/10.1007/s00018-019-03389-7
609 Tang, S., Wang, X., Li, W., Yang, X., Li, Z., Liu, W., Li, C., Zhu, Z., Wang, L., & Wang, J.
610 (2017). Biallelic mutations in CFAP43 and CFAP44 cause male infertility with multiple
611 morphological abnormalities of the sperm flagella. *The American Journal of Human Genetics*
612 *100*(6), 854-864. https://doi.org/10.1016/j.ajhg.2017.04.012
613 Tapia Contreras, C., & Hoyer-Fender, S. (2019). CCDC42 Localizes to Manchette, HTCA and
614 Tail and Interacts With ODF1 and ODF2 in the Formation of the Male Germ Cell Cytoskeleton.
615 *Front Cell Dev Biol 7*, 151. https://doi.org/10.3389/fcell.2019.00151
616 Touré, A., Martinez, G., Kherraf, Z. E., Cazin, C., Beurois, J., Arnoult, C., Ray, P. F., & Coutton,

617 C. (2020). The genetic architecture of morphological abnormalities of the sperm tail. *Hum*
618 *Genet* https://doi.org/10.1007/s00439-020-02113-x

619 Tu, C., Nie, H., Meng, L., Yuan, S., He, W., Luo, A., Li, H., Li, W., Du, J., Lu, G., Lin, G., &
620 Tan, YQ. (2019). Identification of DNAH6 mutations in infertile men with multiple
621 morphological abnormalities of the sperm flagella. *Sci Rep 9*(1), 15864.
622 https://doi.org/10.1038/s41598-019-52436-7

623 Tu, C., Wang, W., Hu, T., Lu, G., Lin, G., & Tan, YQ. (2020). Genetic underpinnings of
624 asthenozoospermia. *Best Pract Res Clin Endocrinol Metab* 101472. https://doi.org/
625 10.1016/j.beem.2020.101472

626 Turner, K. A., Rambhatla, A., Schon, S., Agarwal, A., Krawetz, S. A., Dupree, J. M., & Avidor-
627 Reiss, T. (2020). Male Infertility is a Women's Health Issue-Research and Clinical Evaluation
628 of Male Infertility Is Needed. Cells, 9(4). https://doi.org/10.3390/cells9040990

629 Turner, R. M., Musse, M. P., Mandal, A., Klotz, K., Jayes, F. C., Herr, J. C., Gerton, G. L.,
630 Moss, S. B., & Chemes, H. E. (2001). Molecular genetic analysis of two human sperm fibrous
631 sheath proteins, AKAP4 and AKAP3, in men with dysplasia of the fibrous sheath. *J Androl*
632 *22*(2), 302-315.

633 Tüttelmann, F., Ruckert, C., & Röpke, A. (2018). Disorders of spermatogenesis: Perspectives
634 for novel genetic diagnostics after 20 years of unchanged routine. *Med Genet 30*(1), 12-20.
635 https://doi.org/10.1007/s11825-018-0181-7

636 Wellard, S. R., Hopkins, J., & Jordan, P. W. (2018). A seminiferous tubule squash technique
637 for the cytological analysis of spermatogenesis using the mouse model. *JoVE*(132) e56453.
638 https://doi.org/10.3791/56453

639 Wu, B., Gao, H., Liu, C., & Li, W. (2020). The coupling apparatus of the sperm head and tail.
640 *Biol Reprod 102*(5), 988-998. https://doi.org/10.1093/biolre/ioaa016
641 Zhang, Z., Li, W., Zhang, Y., Zhang, L., Teves, M. E., Liu, H., Strauss, J. F., 3rd, Pazour, G.
642 J., Foster, J. A., Hess, R. A., & Zhang, Z. (2016). Intraflagellar transport protein IFT20 is
643 essential for male fertility and spermiogenesis in mice. *Mol Biol Cell 27*(23), 3705-3716.
644 https://doi.org/10.1091/mbc.E16-05-0318
645 Zhu, F., Liu, C., Wang, F., Yang, X., Zhang, J., Wu, H., Zhang, Z., He, X., Zhang, Z., Zhou,
646 P., Wei, Z., Shang, Y., Wang, L., Zhang, R., Ouyang, Y. C., Sun, Q. Y., Cao, Y., & Li, W.
647 (2018). Mutations in PMFBP1 Cause Acephalic Spermatozoa Syndrome. *Am J Hum Genet*
648 *103*(2), 188-199. https://doi.org/10.1016/j.ajhg.2018.06.010
649 Zhu, F., Wang, F., Yang, X., Zhang, J., Wu, H., Zhang, Z., Zhang, Z., He, X., Zhou, P., Wei,
650 Z., Gecz, J., & Cao, Y. (2016). Biallelic SUN5 Mutations Cause Autosomal-Recessive
651 Acephalic Spermatozoa Syndrome. *Am J Hum Genet 99*(4), 942-949.
652 https://doi.org/10.1016/j.ajhg.2016.11.002
653 Zhu, X., Wang, J., Li, S., Lechtreck, K., & Pan, J. (2020). IFT54 directly interacts with kinesin-
654 II and IFT dynein to regulate anterograde intraflagellar transport. *Embo j*, e105781.
655 https://doi.org/10.15252/embj.2020105781
656 Zinaman, M. J., Brown, C. C., Selevan, S. G., & Clegg, E. D. (2000). Semen quality and human
657 fertility: a prospective study with healthy couples. *J Androl 21*(1), 145-153.
658
659
660

Figures and Figure legends

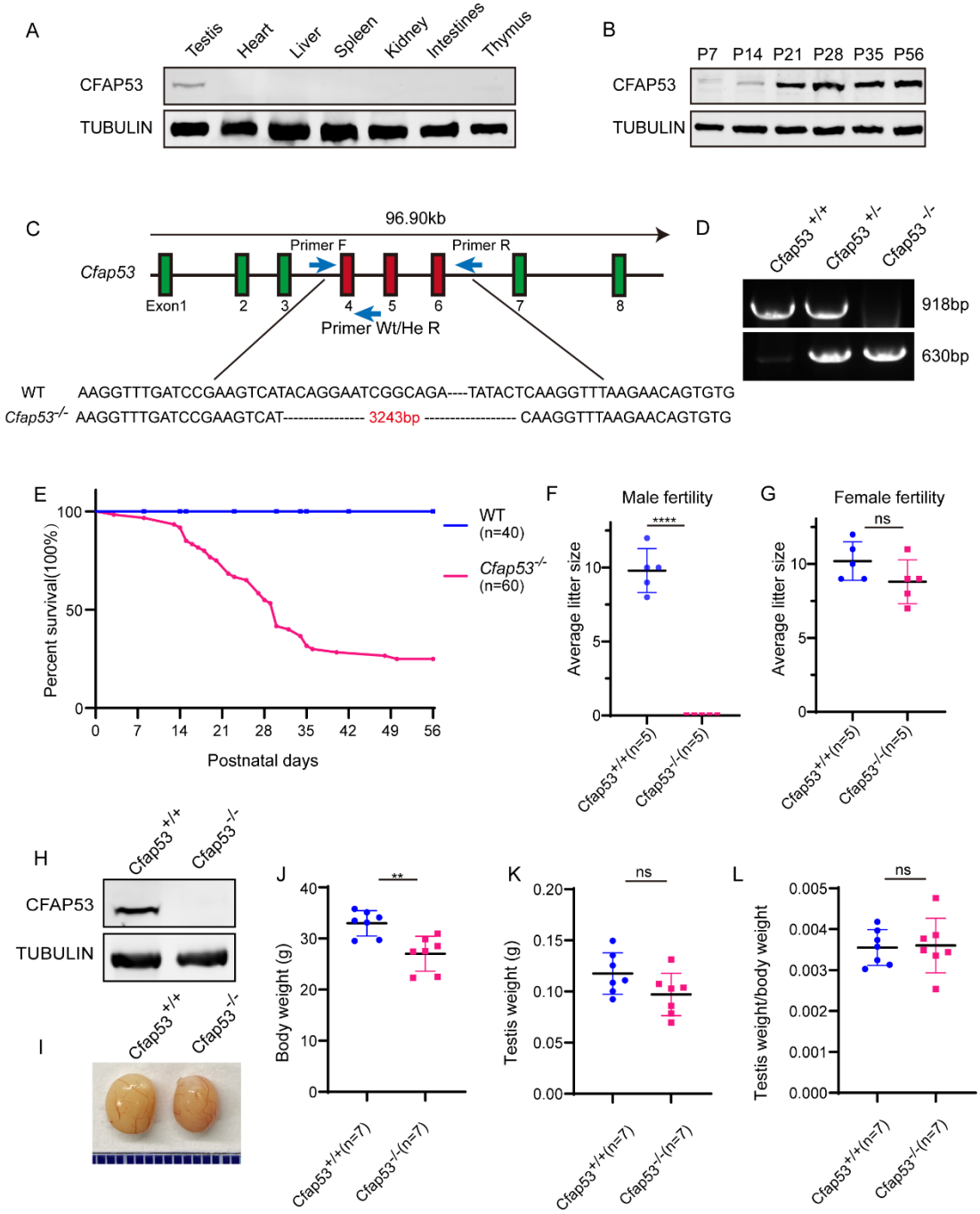

Fig. 1. The generation of *Cfap53* knockout mice. (A) CFAP53 was predominately expressed in testis. Immunoblotting of CFAP53 was performed in testis, heart, liver, spleen, kidney, intestines, and thymus with Tubulin serving as the control. (B) CFAP53 was expressed starting in P7 testes. Tubulin served as the control. (C) The generation of *Cfap53*$^{-/-}$ mice lacking exons 4 to 6. (D) Genotyping of *Cfap53 Cfap53*$^{-/-}$ mice. (E) Survival rate of postnatal *Cfap53*$^{-/-}$ mice

(n = 60). (F) The average litter size of *Cfap53*$^{+/+}$ and *Cfap53*$^{-/-}$ male mice at 3 months (n = 5 independent experiments). *Cfap53*$^{-/-}$ male mice were completely sterile. Data are presented as the mean ± SD. ****$P < 0.0001$. (G) The average litter size of *Cfap53*$^{+/+}$ and *Cfap53*$^{-/-}$ female mice at 3 months (n = 5 independent experiments). *Cfap53*$^{-/-}$ female mice were fertile. Data are presented as the mean ± SD. (H) Immunoblotting of CFAP53 in *Cfap53*$^{+/+}$ and *Cfap53*$^{-/-}$ testes. Tubulin served as the control. (I) The testis sizes of *Cfap53*$^{+/+}$ and *Cfap53*$^{-/-}$ mice were similar to each other. Data are presented as the mean ± SD. (J) The body weights of *Cfap53*$^{-/-}$ male mice were lower compared to *Cfap53*$^{+/+}$ male mice (n = 7 independent experiments). Data are presented as the mean ± SD. **$P < 0.01$. (K) The testis weights of *Cfap53*$^{+/+}$ and *Cfap53*$^{-/-}$ male mice (n = 7 independent experiments). Data are presented as the mean ± SD. (L) The ratio of testis weight/body weight in *Cfap53*$^{+/+}$ and *Cfap53*$^{-/-}$ male mice (n = 7 independent experiments). Data are presented as the mean ± SD.

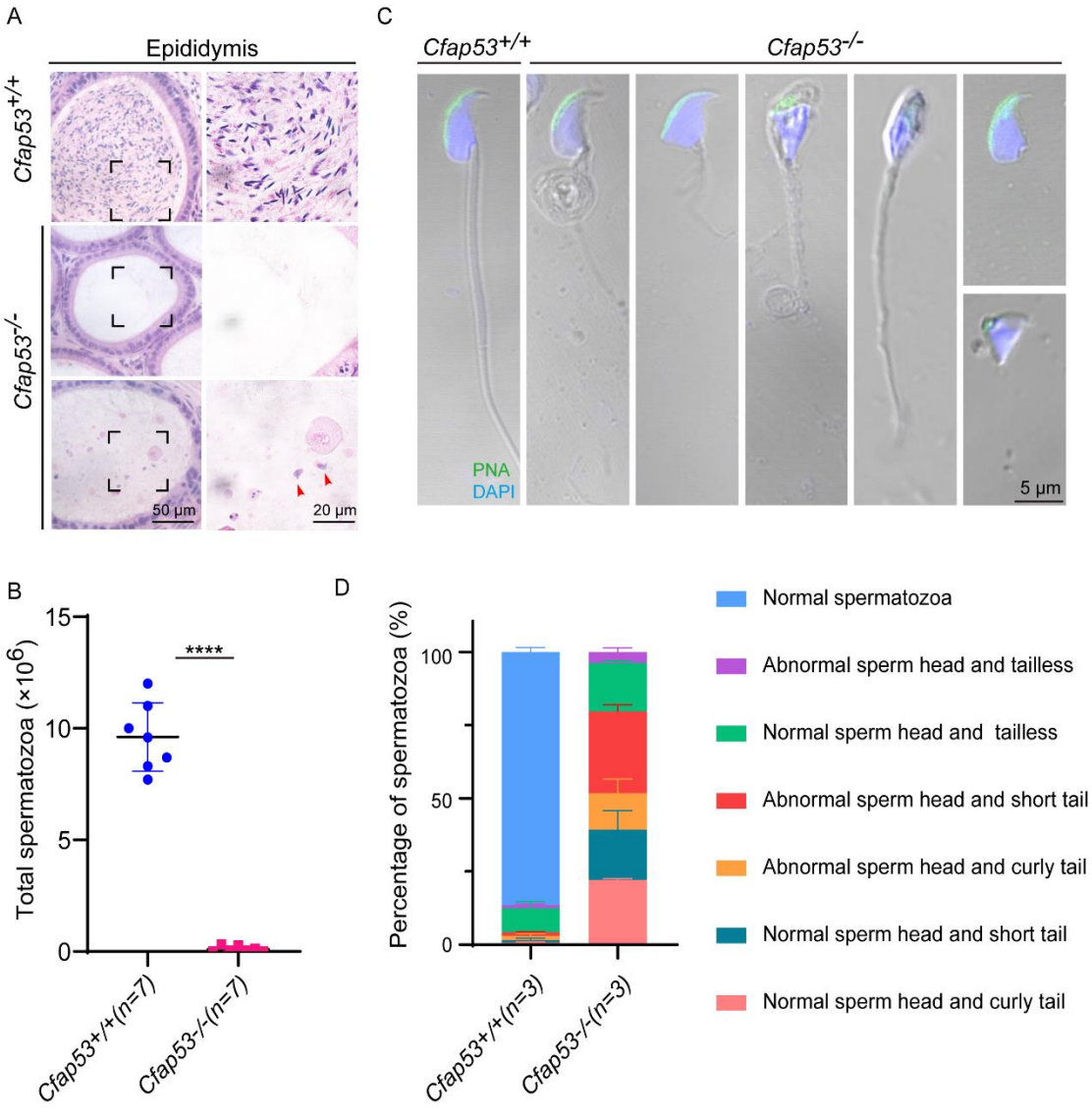

Fig. 2. CFAP53 knockout results in MMAF. (A) H&E staining of the caudal epididymis from *Cfap53*$^{+/+}$ and *Cfap53*$^{-/-}$ male mice. (B) The sperm counts in the caudal epididymis were significantly decreased in the *Cfap53*$^{-/-}$ male mice (n = 7 independent experiments). Data are presented as the mean ± SD. ****$P < 0.0001$. (C) Immunofluorescence staining of PNA in Cfa*p53*$^{+/+}$ and *Cfap53*$^{-/-}$ spermatozoa, indicating abnormal spermatozoa such as abnormal head and coiled, short, or absent flagella. (D) Quantification of different categories of abnormal spermatozoa (n = 3 independent experiments). Data are presented as the mean ± SD. The statistical significance of the differences between the mean values for the different genotypes

689 was measured by Student's t-test with a paired 2-tailed distribution.

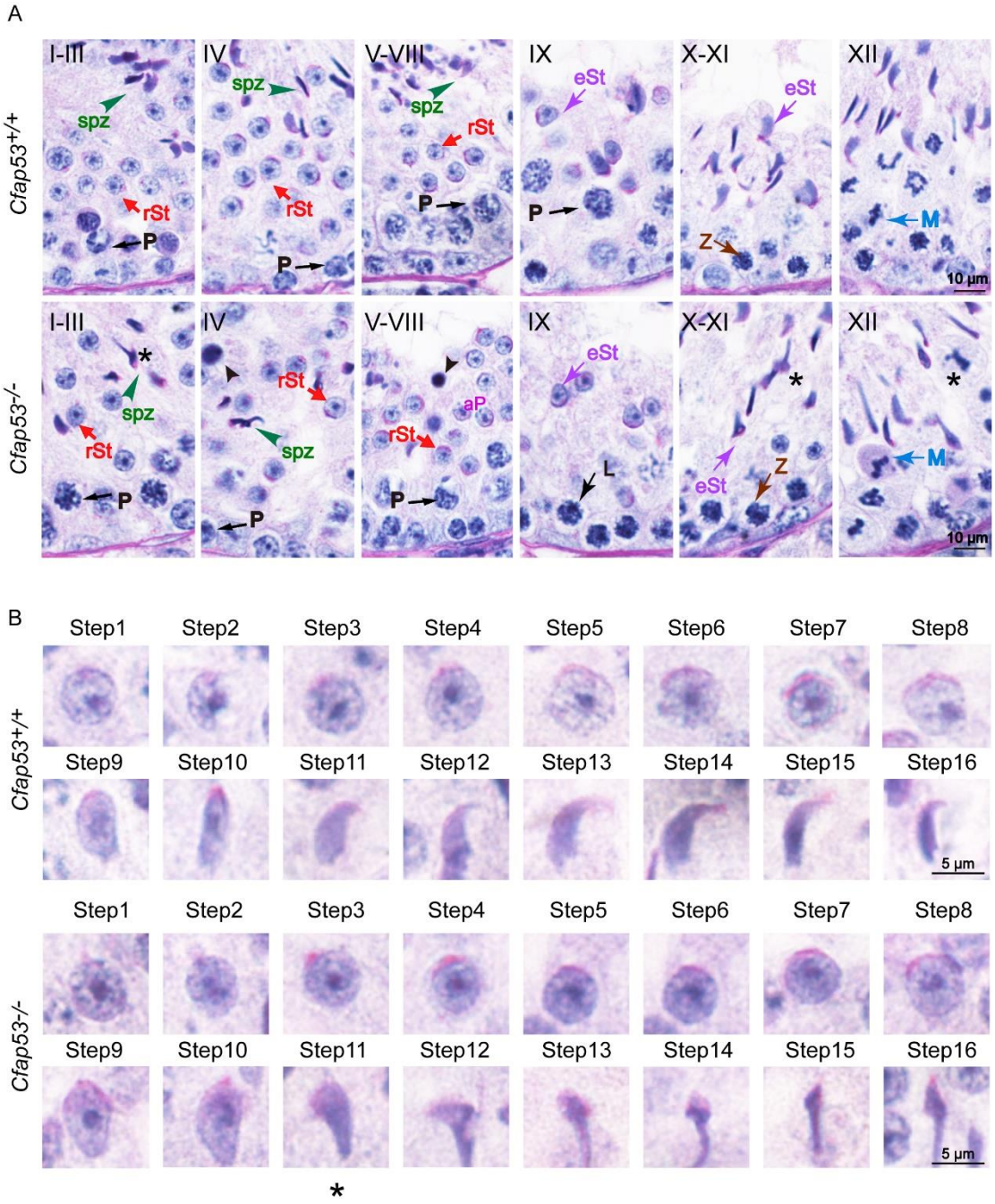

690

691 **Fig. 3. Spermatogenesis defects of *Cfap53*$^{-/-}$ mice.** (A) PAS staining of testes sections from

692 *Cfap53*$^{+/+}$ and *Cfap53*$^{-/-}$ mice. Defects in the nuclear shape of several elongating spermatids

693 were clearly evident in the *Cfap53*$^{-/-}$ seminiferous tubule (asterisks). Apoptotic bodies were

694 detected in *Cfap53*$^{-/-}$ testes sections (black arrowheads). P: pachytene spermatocyte, L:

695 leptotene spermatocyte, Z: zygotene spermatocyte, M: meiotic spermatocyte, rST: round

696 spermatid, eST: elongating spermatid, spz: spermatozoa. (B) The PAS staining of spermatids at

697 different steps from *Cfap53*$^{+/+}$ and *Cfap53*$^{-/-}$ mice. From step 1 to step 10 spermatids, the head

698 morphology was roughly normal in *Cfap53*$^{-/-}$ mice. Abnormal, club-shaped heads (asterisk)

699 were first seen in step 11 spermatids in *Cfap53*$^{-/-}$ mice.

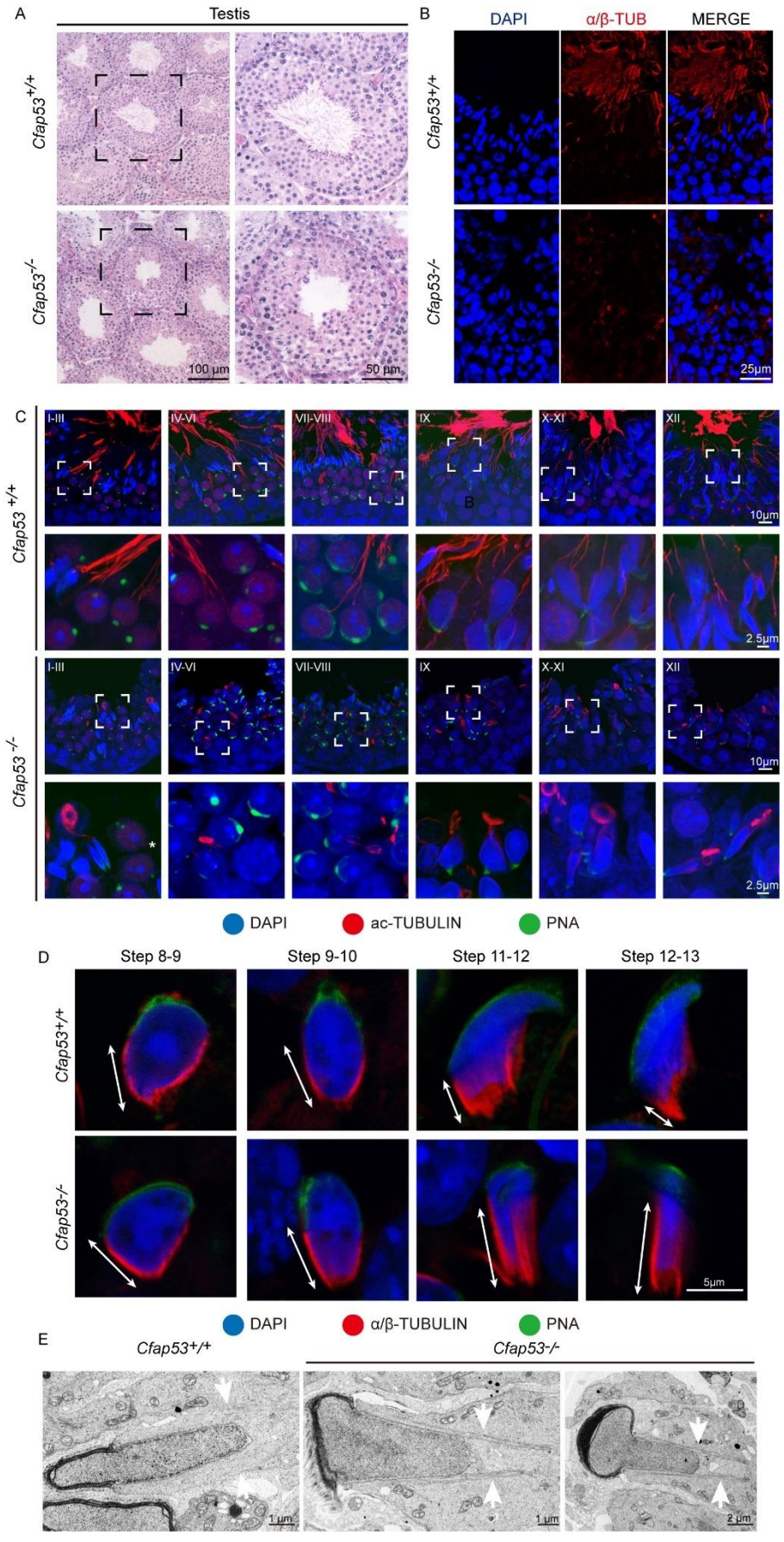

700

Fig. 4. Sperm flagellum biogenesis defects and abnormal manchettes in *Cfap53*$^{-/-}$ mice. (A) H&E staining of testes sections from *Cfap53*$^{+/+}$ and *Cfap53*$^{-/-}$ male mice. (B) Immunofluorescence of anti-α/β-tubulin (red) antibodies in testes sections from *Cfap53*$^{-/-}$ male mice show flagellar defects. (C) Comparison of flagellum biogenesis in testes sections from *Cfap53*$^{+/+}$ and *Cfap53*$^{-/-}$ mice at different stages. Sperm flagella were stained with acetylated Tubulin (red), the acrosome was stained with PNA lectin histochemistry (green), and the nucleus was stained with DAPI (blue). Flagellum formation was first observed at stages I-III of the seminiferous epithelial cycle in *Cfap53*$^{+/+}$ mice, while sperm tails were not detected (asterisks) at stages I-III in testes sections in *Cfap53*$^{-/-}$ mice. From stages IV–VI, sperm flagellum biogenesis defects were clearly seen in *Cfap53*$^{-/-}$ testis sections. (D) Comparison of manchette formation between *Cfap53*$^{+/+}$ and *Cfap53*$^{-/-}$ spermatids at different steps. The manchette was stained with α/β-tubulin (red), the acrosome was stained with PNA lectin histochemistry (green), and the nucleus was stained with DAPI (blue). The distance from the perinuclear ring to the caudal side of the nucleus is indicated by white arrows. During steps 12 and 13, the distance was reduced in *Cfap53*$^{+/+}$ spermatids, while the manchette of *Cfap53*$^{-/-}$ spermatids displayed abnormal elongation. (E) Transmission electron microscope images of *Cfap53*$^{-/-}$ step 11–13 spermatids showing the perinuclear ring constricting the sperm nucleus and causing abnormal sperm head formation. White arrows indicate the manchette microtubules.

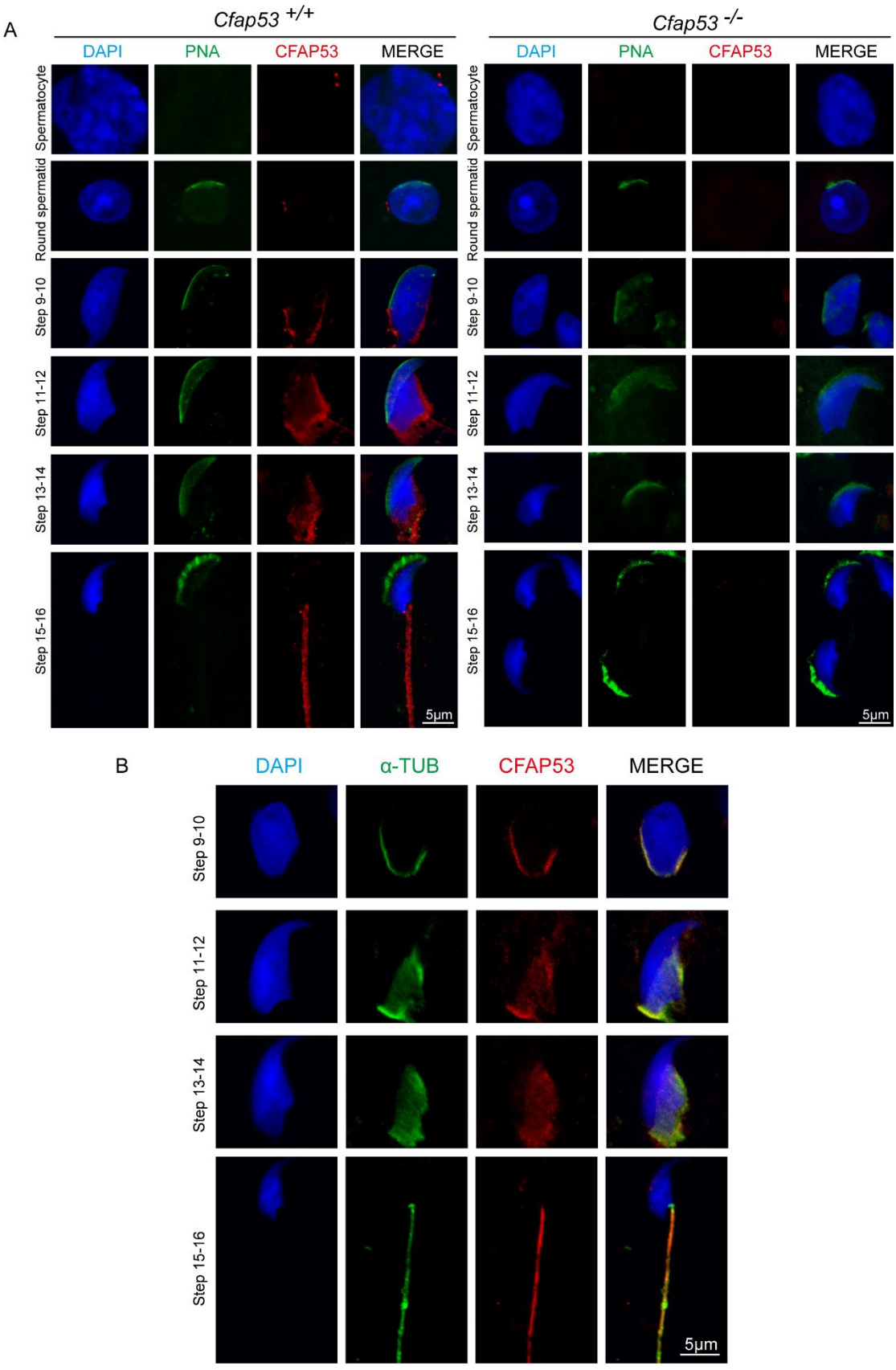

Fig. 5. Localization of CFAP53 in developing germ cells. (A) Testicular germ cells were prepared from *Cfap53*$^{+/+}$ and *Cfap53*$^{-/-}$ adult mouse testis, and immunofluorescence staining

723 was performed with antibodies to CFAP53 (red). The acrosome was stained with PNA lectin
724 histochemistry (green), and the nucleus was stained with DAPI (blue). (B) Testicular spermatids
725 of WT adult mouse testes were stained with antibodies against α-tubulin (green) and CFAP53
726 (red). The nucleus was stained with DAPI (blue). In step 9–14 spermatids, CFAP53 was
727 detected at the manchette. In 15–16 spermatids, CFAP53 was located at the sperm tail.

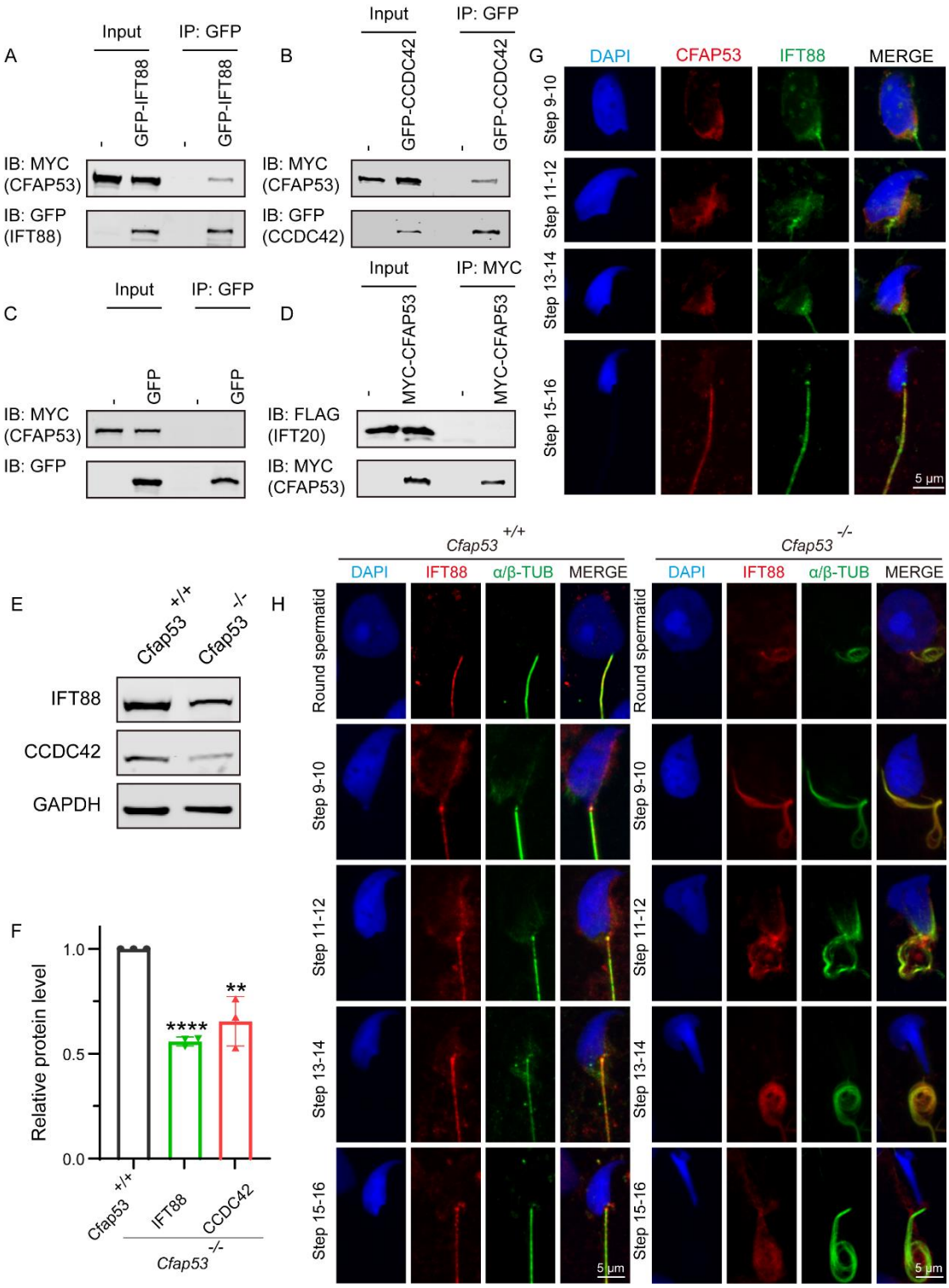

Fig. 6. CFAP53 interacts with IFT88 and CCDC42. (A) and (B) CFAP53 interacts with IFT88 and CCDC42. *pCS2-Myc-Cfap53* and *pEGFP-GFP-Ift88* or *pEGFP-GFP-Ccdc42* were co-transfected into HEK293T cells. At 48 h after transfection, the cells were collected for immunoprecipitation (IP) with anti-GFP antibody and analyzed with anti-MYC and anti-GFP

antibodies. (C) *pCS2-Myc-Cfap53* and Empty vector were co-transfected into HEK293T cells. At 48 h after transfection, the cells were collected for IP with anti-GFP antibody and analyzed with anti-MYC and anti-GFP antibodies. (D) *pCS2-Myc-Cfap53* and *pRK-Flag-Ift20* were co-transfected into HEK293T cells. At 48 h after transfection, the cells were collected for IP with anti-MYC antibody and analyzed with anti-MYC and anti-FLAG antibodies. (E) Western blot analysis showing IFT88 and CCDC42 protein levels in $Cfap53^{+/+}$ and $Cfap53^{-/-}$ mouse testis lysates. GAPDH served as the loading control. (F) Quantification of the relative protein levels of IFT88 and CCDC42 using the Odyssey software and compared with the control group (n = 3 independent experiments). Data are presented as the mean ± SD. The statistical significance of the differences between the mean values for the different genotypes was measured by Student's t-test with a paired, 2-tailed distribution. $^{**}P < 0.01$ and $^{****}P < 0.0001$. (G) The immunofluorescence analysis of IFT88 (green) and CFAP53 (red) was performed in testicular germ cells. The nucleus was stained with DAPI (blue). (H) Immunofluorescence staining with antibodies against IFT88 (red) and α/β-tubulin (green) in spermatids at different developmental stages from $Cfap53^{+/+}$ and $Cfap53^{-/-}$ adult mice. The nucleus was stained with DAPI (blue).

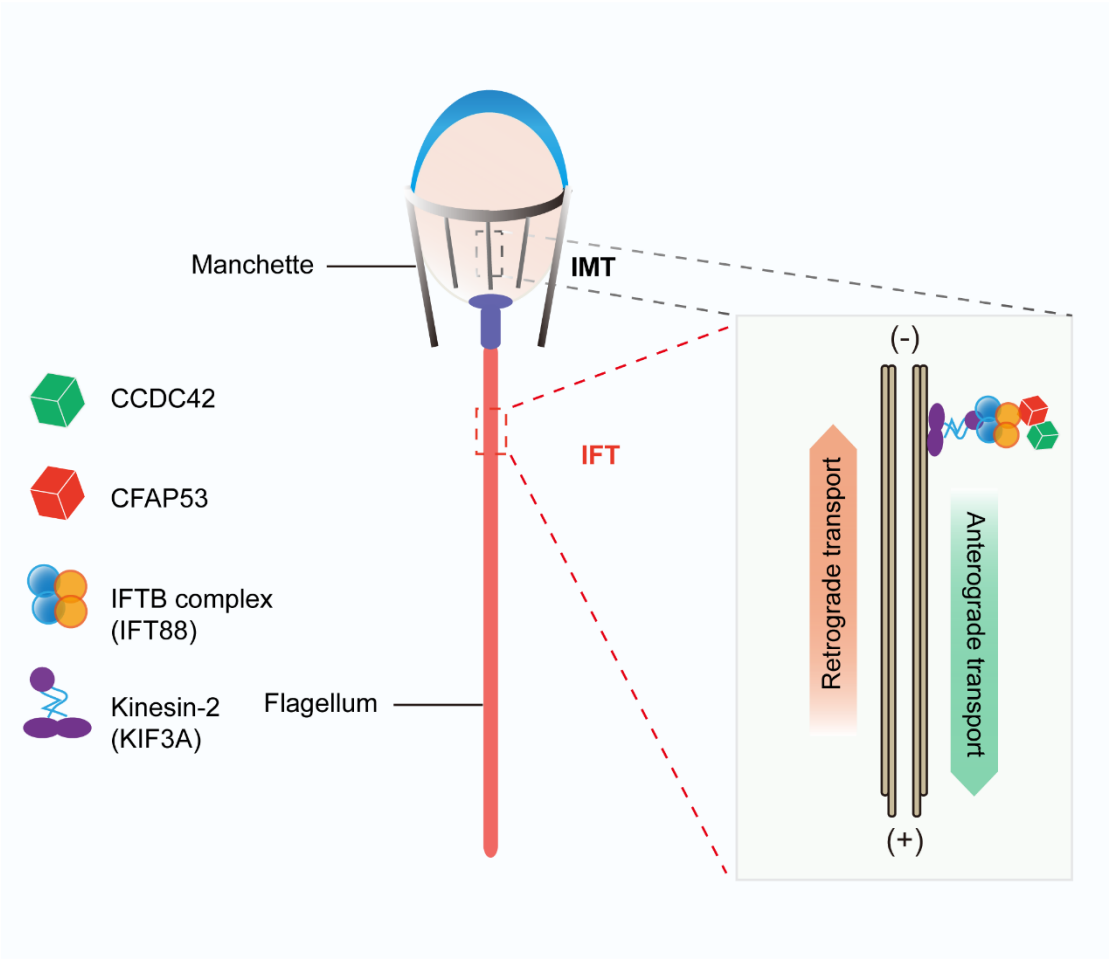

748

749 **Fig. 7. Proposed model for the functional role of CFAP53 during flagellum biogenesis.**

750 CFAP53 works as a cargo protein, and it is involved in the stabilization of other cargo proteins,

751 such as CCDC42, that need to be transported to the developing sperm tail. During transport,

752 CFAP53 interacts with IFT complex B member IFT88 and kinesin-2 motor subunit KIF3A for

753 targeting to its destination.

A

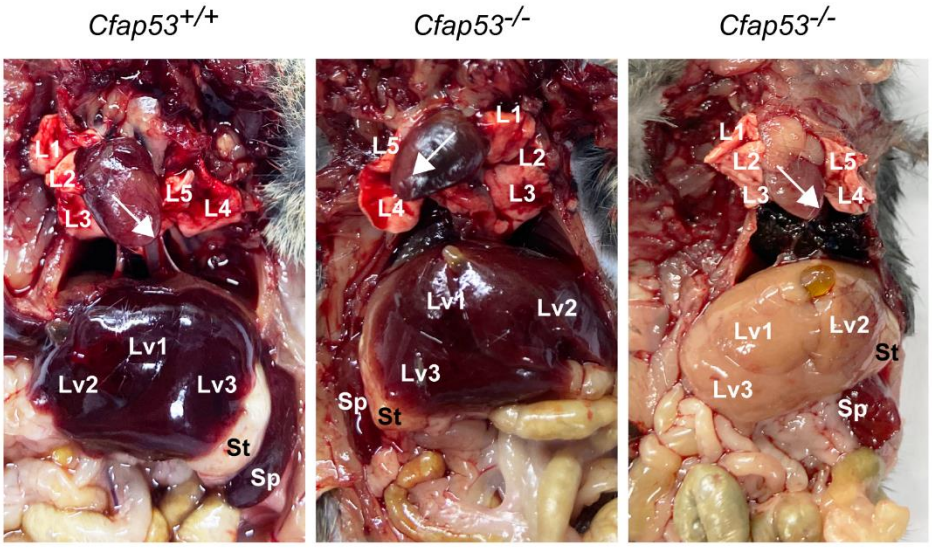

B

ID	Brain	Situs	Heart	Liver	Spleen
1	Hydrocephalus	SIT	Dextrocardia	Inverted	Abcent
2	Hydrocephalus	SS	Levocardia	Normal	Normal
3	Hydrocephalus	SS	Levocardia	Normal	Normal
4	Hydrocephalus	SS	Levocardia	Normal	Normal
5	Hydrocephalus	SS	Levocardia	Normal	Normal
6	Hydrocephalus	SS	Levocardia	Normal	Normal
7	Normal	SIT	Dextrocardia	Inverted	Inverted
8	Hydrocephalus	SIT	Dextrocardia	Inverted	Inverted
9	Hydrocephalus	SIT	Dextrocardia	Inverted	Inverted
10	Normal	SIT	Dextrocardia	Inverted	Inverted
11	Normal	SIA	Levocardia	Inverted	Splitted
12	Normal	SIA	Levocardia	Inverted	Inverted
13	Normal	SIT	Dextrocardia	Inverted	Abcent
14	Normal	SIT	Dextrocardia	Inverted	Inverted
15	Normal	SIT	Dextrocardia	Inverted	Inverted
16	Normal	SIT	Dextrocardia	Inverted	Inverted
17	Normal	SIT	Dextrocardia	Inverted	Inverted
18	Normal	SIT	Dextrocardia	Inverted	Inverted
19	Normal	SIT	Dextrocardia	Inverted	Inverted

754

Supplementary Figure 1. Left-right body asymmetry defects and hydrocephalus in *Cfap53*$^{-/-}$ mice. (A) *Cfap53*$^{-/-}$ mice presented with situs inversus totalis (SIT), situs inversus abdominalis (SIA), and situs solitus (SS). L1-5 (white numbers): lung lobes, Lv1-3 (white numbers): liver lobes, St: stomach, Sp: spleen. (B) Summary of the phenotypes detected in *Cfap53*$^{-/-}$ mice.

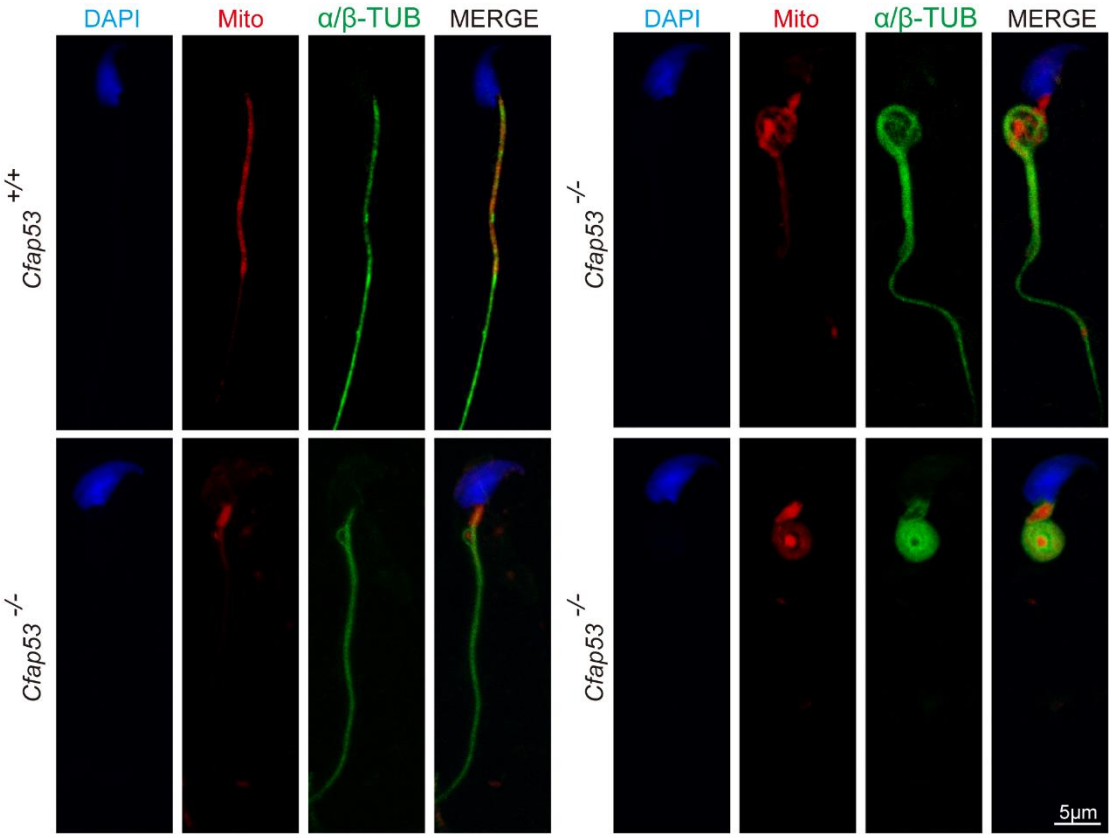

Supplementary Figure 2. Mitochondrial sheath defects in *Cfap53*$^{-/-}$ spermatozoa. The immunofluorescence analysis for α/β-tubulin (green) and MitoTracker (red) was performed in *Cfap53*$^{+/+}$ and *Cfap53*$^{-/-}$ spermatozoa. The nucleus was stained with DAPI (blue).